Electrospun core-sheath PAN@PPY nanofibers decorated with ZnO: Photo-induced water decontamination enhanced by a semiconducting support

Electrospun core-sheath PAN@PPY nanofibers decorated with ZnO: photo-induced water decontamination enhanced by formation of a heterojunction

Gabriele Capilli, Paola Calza, Claudio Minero, Marta Cerruti

Mining & Materials Engineering, McGill University, 3610 University Street, Montreal, Quebec H3A 0C5, Canada

Dipartimento di Chimica, Università degli Studi di Torino – via Pietro Giuria 5, 10125 Torino, Italy

KEYWORDS electrospinning, conducting polymer, semiconducting nanofibers, polypyrrole, heterojunction, Zinc Oxide, photocatalysis, water treatment, AOP

ABSTRACT

We built a photoactive system for water decontamination, consisting in ZnO nanocrystals supported on a flexible mat of electrospun semiconducting nanofibers. The synthesized nanofibers own a core-sheath structure, with a polyacrylonitrile (PAN) core and a sheath made of polypyrrole (PPY), a conducting polymer, actually a low band gap p-type semiconductor. Under UVA irradiation, the heterojunction formed between PPY and ZnO, a n-type semiconductor, promotes the separation of the charge carriers photogenerated at the interface. Their consequent lower recombination rate results in a higher photocatalytic efficiency – assessed through photodegradation of Methyl Orange – compared to a combined system based on an insulating support (bare PAN nanofibers). UV-Vis photoactive metal oxide nanoparticles have been already immobilized on insulating supports, to avoid the expensive separation and collection of the suspended nanocatalyst, at the end of the water treatment. Here we show how a semiconducting support represents a solution not only to the not scalable nanofiltration but also to increase photocatalytic efficiency, thanks to its 'active' role. To build the combined system, we first electrospun the insulating PAN core, chemically inert and with high tensile strength. On the PAN mat we then formed the semiconducting layer, through polymerization of pyrrole in water solution. Finally, we decorated the core-sheath mat with a steady coverage of ZnO nanocrystals, through a two-steps method: a seeding step with a Zn-containing precursor, followed by a growing step, a hydrothermal treatment at very low temperature (90°C), to preserve the polymeric support.

INTRODUCTION

Advanced methods for water decontamination usually employ materials exhibiting a catalytic activity under UV-Vis light (called photoactive), because of their degradation action without needing any addition of chemicals.[1,2] The materials studied are mostly metal oxides[3,4], in the form of nanopowders suspended in the treatment solution. TiO_2[5,6] is far the most famous oxide for these applications, due to its many positive features including superior photocatalytic efficiency, photostability, low cost preparation and highly oxidizing photogenerated holes. Recently, some interest has increased also for ZnO.[7,8] It owns most of the

positive properties of TiO_2, moreover it is possible to obtain ZnO crystalline phases (fundamental to observe photoactivity), with multiple shape and size[9], even in mild synthetic conditions.[10,11]

Nowadays, water treatments employing photoactive nanomaterials are still prevented to scale up to the wide world level.[12,13] The efficiency of the process, the conversion of photons in active chemical species able to degrade pollutants, needs to increase.[14] Moreover, the nanoparticle collection (through nanofiltration) at the end of the treatment is not sustainable on a large scale.[15,16]

Immobilization of nanoparticles onto a mechanically resistant solid support, i.e. a polymeric membrane[17], a mat of nanofibers[18], represents a solution to the second issue. Flexible supports with high surface area are frequently fabricated through electrospinning, a user-friendly, scalable technique, capable to produce a continuous nanometric polymeric fiber.[19] Electrospun nanofibers coated with a metal oxide layer, to form a core-sheath structure, have already been adopted for multiple purposes, ranging from optoelectronics[20], to energy storage[21], to sensing[22], to environmental applications.[23-25]

In all these cases the supporting material is electrically insulating and contributes just to the mechanical properties of the combined system, not to its activity. Contrarily, a semiconducting support is expected to increase the overall photoactivity, thanks to the formation of a heterojunction at the interface between the two phases (support and oxide coating).[26-28] The permanent electric field established in the thin p-n heterojunction promotes the separation of the photoinduced charge carriers, suppressing their recombination through their selective collection: electron on the n-type material and holes on the p-type one. Coupling metal oxides (typically n-type semiconductors) and conducting polymers (usually p-type semiconductors with band gap width depending on their doping grade[29,30]), in the form of core-shell nanoparticles[31] or nanofilms[28,32], has already widely proved an enhancement in photocatalytic activity, due to the development of a heterojunction.

Here we report a composite system for water decontamination applications, which combines an electrospun semiconducting polymeric support with a ZnO photoactive coating (see Fig. 1), to generate a heterojunction. Our approach tries to overcome the expensive separation of photoactive nanoparticles from purified water and to satisfy the need of higher photoactivity, at the same time.

Specifically, the support consists in a mat of core-sheath nanofibers, with an insulating core of polyacrylonitrile (PAN) and a semiconducting sheath of polypyrrole (PPY). Examples of similar electrospun fibers are available in literature.[33,34] The intrinsic high crystalline behaviour of a pure conducting polymer prevents its direct electrospinning[35,36]: its ordered domains are almost insoluble in any solvent used for electrospinning, leading to a low processing ability. Whenever conducting fibers are obtained, they would be fragile.[34,37] It is possible to blend the conducting polymer with electrospinnable additives, but the resulting electrospun fibers would own a remarkably lower electrical conductivity.[35,38]

PAN is easily electrospinnable, it exhibits high tensile strength in addition to high chemical and thermal stability[24,39], which make it resistant to degradation even under hydrothermal conditions. Among the conducting polymers, PPY seems the best compromise in terms of cost of preparation, conductivity, stability in the photodegradation conditions and low response to acid/base doping, especially if doped with big organic counterions.[40-42] Crystalline ZnO nanoparticles must be obtained in mild conditions (primarily low T), in order to preserve the flexibility and conductivity of the polymeric nanofibers.[25,43] Since the conventional approaches to convert the precursors in crystalline metal oxides, i.e. calcination[44] and hydrothermal treatment (HT)[44,45], require too high temperatures, they are forbidden in this case.

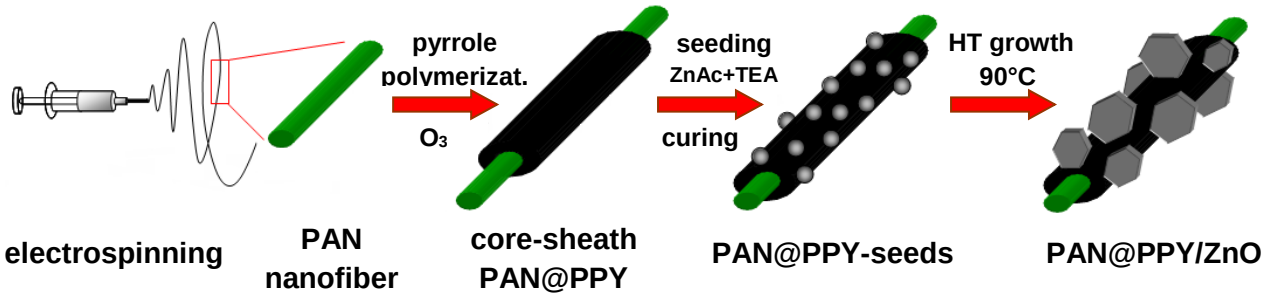

Figure 1: Schematic production of core-sheath PAN@PPY nanofibers decorated with ZnO nanocrystals.

MATERIALS AND METHODS

Chemicals and Materials

Pyrrole (Py) 98%, ammonium peroxydisulfate (APS), 4-dodecylbenzene sulfonic acid (DBSA) 99%, zinc acetate dehydrate (ZnAc), triethylamine (TEA), zinc nitrate hexahydrate (ZnNIT), hexamethylenetetramine (HMTA), Methyl Orange (MO) were purchased from Sigma Aldrich. PAN (MW: 50,000-70,000 Da, 99%) was supplied by Sarchem Laboratories Inc (New Jersey), dimethylformammide (DMF) and isopropyl alcohol (IPA) by Fisher Scientific. All the chemicals were used without any further purification. Water employed was purified with a MilliQ plus apparatus (TOC = 2 ppb, conductivity 18.2 MΩ cm).

Electrospinning of PAN nanofibers

We electrospun the PAN nanofibers with an E200 electrospinning device (Inovenso, Turkey), using a solution of PAN in DMF 20% w/w (see more details in SI). We then treated the electrospun mats in an UV-ozonolysis machine (UVO cleaner mod. 42A, Jelight, USA), for 3.5 minutes on both sides, in order to enhance the hydrophilicity of PAN.

Preparation of core-sheath PAN@PPY nanofibers

To carry out the Py polymerization, we first prepared 10 ml of water solution containing Py (0.0335 g, 50 mM) and the dopant, DBSA (0.1632 g, 50 mM) and kept it at 4-5°C, under stirring. We then prepared a second solution by dissolving a strong oxidant, APS (0.1141 g, 100 mM), in 5 ml of water and added it dropwise (1 ml min^{-1}) to the former one, under vigorous stirring, in ice bath. After complete APS addition, we kept the polymerizing solution at 4-5°C for one hour before carrying out the first impregnation cycle. We laid down the PAN mats horizontally on a Parafilm support and impregnated them drop by drop with the polymerizing solution (on average 0.15 ml cm^{-2} each cycle). We kept both the PPY solution and the impregnated mats at 4-5°C during the entire process, to slow down the Py polymerization. We let the mats dry naturally each time, before repeating the impregnation procedure. We impregnated the nanofibers three more times to obtain the 'PAN@PPY' mats: after 4 h and 7 h from APS addition and finally with a new PPY solution, again after 7 h polymerization (that is, after APS addition) (see Fig. S3).

Preparation of ZnO coated PAN@PPY nanofibers

Seeding step

We prepared the ZnO seeding suspension following a procedure in literature.[43] We first dissolved 1.10 g (5 mmol) of ZnAc in IPA (50 ml). After heating the solution at 85°C for 20 min, under vigorous stirring, it turned in a white opaque colloid. We then stopped heating and added 0.7 ml of TEA (5 mmol) dropwise, under continuous stirring. The colloid turned to a clear solution. We heated again the solution at 85°C for 10 min, while stirring and a white colloid formed again. We finally cooled the seeding suspension to room T and incubated it without stirring for 2 h, before use in the impregnation cycles. It remained stable up to two weeks, after then progressive particle growth and settling began and we needed to prepare a new suspension. During the impregnation cycles, we laid the PAN@PPY mats on a Parafilm support and added the seeding suspension drop by drop (on average 0.25 ml cm^{-2} each cycle). We let them dry naturally at room T (it took 20-30 min) and repeated the impregnation-drying cycle 4 times. We finally cured them in air at 100°C, for 1 h to promote the seed fixation (by formation of chemical bonds with PPY) on the mats, named 'PAN@PPY-seeds'.

Hydrothermal growing

Following previous works[24,25,43], we soaked one PAN@PPY-seeds mat (2x3 cm) in 70 ml of a just prepared equimolar (50 mM) aqueous solution of ZnNIT and HMTA. We immobilized the mat on a glass slide to keep it immersed, on the bottom of the 100 ml Teflon inner. It underwent mild HT (90°C for 5 h, in a sealed stainless steel autoclave), to convert the seeds in ZnO nanocrystals, then naturally cooled down to room T. We repeatedly rinsed the resulting mat, named 'PAN@PPY/ZnO', with water before drying in vacuum at room T.

Synthesis of reference materials

We prepared the 'PAN/ZnO' sample by treating the PAN mat directly with the seeding and HT steps, without the PPY coating. We obtained the 'Zn-seeds' powder after drying 50 ml of seeding suspension in oven (70°C) and subsequent curing air at 100°C, for 1 h. We referred to 'ZnO_HT90' to indicate the powder obtained after HT of the Zn-seeds powder at 90°C, in the growing solution. We also synthesized a benchmark photocatalytic ZnO nanopowder, called 'ZnO_HT180', by HT at 180°C, overnight, of a ZnNIT solution 0.1 M at pH = 11 (by addition of NaOH). After HT, we washed the settled powder three times with water and collected it by centrifugation, before drying at 70°C overnight.

Characterization

The mat surface was observed using an Inspect-F50 field emission scanning electron microscope (FE-SEM) (FEI, Japan), equipped with an EDAX Octane Super 60 mm 2ndSDD and TEAM EDS analysis system. Samples were coated with a 5 nm Pt layer by using a LEICA EM ACE600 sputtering machine. Electrical conductivity measurements were carried out with a four-point probe. The reported values refer to the whole mats (thickness between 0.1 to 0.05 mm), not to the PPY coating (< 1 µm). Diffuse reflectance spectra were recorded using a dual-beam Varian Cary 5000 UV-Vis-NIR Reflectance Spectrophotometer, with an integrating sphere. The internal walls of the integrating sphere were coated with PTFE and $BaSO_4$ was used as reference material. X-ray diffraction (XRD) patterns were recorded using a Bruker D5000 diffractometer working in Bragg-Brentano configuration, with a Cu anode as X-rays source (Cu–K_α radiation = 0.15418 nm), operating at 40 kV accelerating voltage and 30 mA applied current. Samples were hosted on a flat amorphous SiO_2 holder.

The photodegradation measurements were carried out under UVA irradiation, overnight, using a Philips PL-S 9W/2P BLB fluorescent lamp (Eindhoven, Nederland), with a narrow emission spectrum at 350-

400 nm. We employed cylindrical Pyrex cells (4.0 cm diameter and 2.5 cm height) containing 5 ml of MO aqueous solution (10^{-4} M) and one string (1.5 x 0.5 cm) of photocatalytic mat. The solutions were not stirred and were left in dark for 2 hours, before irradiation, to achieve the adsorption-desorption equilibrium between substrate and photocatalyst. After irradiation, the solution absorption was analyzed with a Varian CARY 100 UV-Vis spectrophotometer (Agilent, CA, USA). Photocatalytic benchmark tests were also carried out on suspensions of ZnO_HT180 nanopowder (0.5 g dm^{-3}), in the presence of the same concentration of MO. During irradiation the slurries were magnetically stirred and after irradiation they were filtered through a 0.45 µm hydrophilic PTFE membrane, to eliminate the ZnO nanoparticles before UV-Vis absorption measurement.

The electrochemical measurements were carried out with a computer-controlled potentiostat (PGSTAT12, Autolab) and a standard three-electrode cell. The working electrodes (WE) consisted in ITO covered with a thin layer of the material under investigation, prepared via doctor blade technique, in the case of Zn-seeds and ZnO_HT90 powders. The ITO/PPY WE were prepared after 4 subsequent depositions of the Py polymerizing solution on a ITO conducting support, lying horizontally, as described for the preparation of PAN@PPY. Ag/AgCl/KCl (3 M) was the reference electrode (RE) and a Pt sheet the counter electrode (CE). The electrolytic solution was aqueous 0.1 M KNO_3, purged with N_2 and a 150 W Xe arc lamp was the light source (LOT Oriel).

RESULTS AND DISCUSSION

PAN@PPY nanofibers

The first step of our procedure, as illustrated in Fig. 1, consists in electrospinning the PAN core and subsequent coating with a semiconducting PPY sheath. Fig. 2 shows the evolution of PAN nanofibers after PPY coating. The white PAN mat (Fig. 2A, inset) is composed of smooth monodispersed fibers with average diameter of 550 ± 50 nm. After four PPY deposition cycles, it exhibits a homogeneous black-dark green colour (Fig. 2B, inset). The nanofibers result covered by a continuous PPY coating, stable after washing (Fig. S3). Their surface appears rough (Fig. 2B), showing the presence of PPY domains. The average fiber thickness increases, and so does the standard deviation: 780 ± 350 nm.

The mat conductivity (Fig. 2C) goes from below the detection limit, in the case of PAN, to 10.3 ± 2.0 10^{-3} S cm^{-1}, for PAN@PPY. These values refer to volumetric conductivities: the sample thickness includes both the non-conductive PAN and conductive PPY layers. The specific electrical conductivity of the PPY sheath is remarkably higher and cannot be uniquely identified.[38] The lack of a continuous contact between the PPY domains, on the fibers, leads to negligible electrical conductivity on a macroscopic scale.[35,46] PAN@PPY conductivity is only marginally larger, compared to that measured on PAN mats coated with only two PPY impregnation cycles (7.7 ± 1.1 10^{-3} S cm^{-1}, see Fig. S4). This evidence indicates that a continuous PPY coating has already formed after 2 cycles even if the mat colour has not turned dark yet (Fig. S3).

Diffuse reflectance measurements carried out on the PAN@PPY mats (Fig. 2D and Fig. S5) reveal a large absorption increase in the whole UV-Vis-NIR range, compared to PAN, further proving the presence of a low band gap semiconducting layer. EDS on the fibers is also able to recognise the PPY coating (Fig. 2E, see also Fig. S6). Since the same elements (H, C, N), almost in the same ratio, are present both in PPY and PAN, PPY is indirectly identified by the increase of oxygen and the appearance of sulphur on the PAN@PPY sample, coming from the dopant (DBSA, a sulfonic acid).

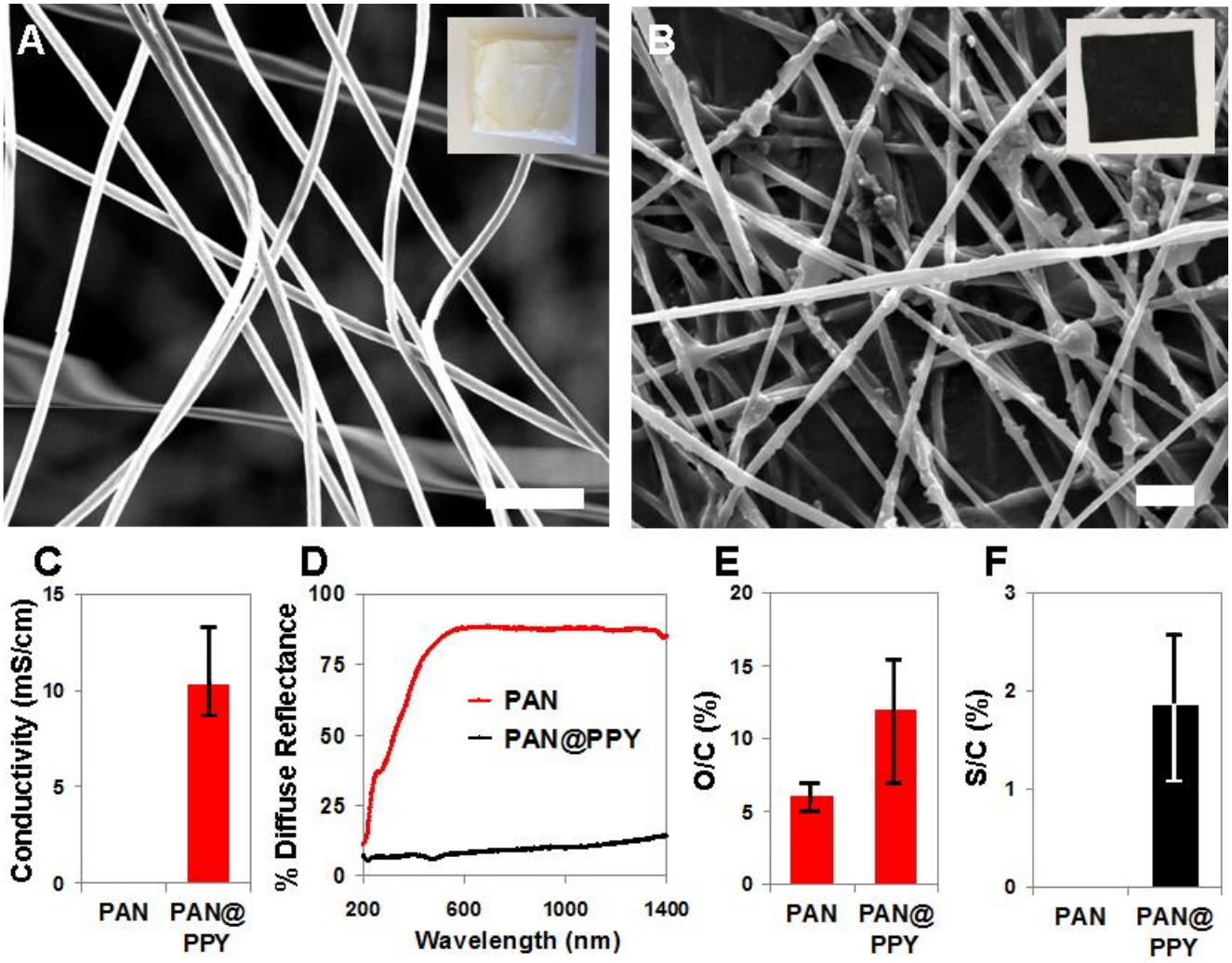

Figure 2: SEM micrographies of PAN (A) and PAN@PPY nanofibers (B). Scale bars: 5 µm. Insets: digital pictures of the corresponding mats. Physicochemical properties of PAN and PAN@PPY mats, including electrical conductivity (C) and absorption in the UVA-Vis-NIR region (D). O/C and S/C elemental ratios in PAN and PAN@PPY nanofibers, measured by EDS (E, F).

A fast ozone treatment, carried out on the electrospun PAN mat, dramatically increases the surface concentration of hydrophilic groups on the fibers. The Py polymerization solution easily impregnates the hydrophilic functionalized nanofibers and the forming PPY domains strongly adhere on PAN (Fig. S1). Ozonation is essential to let the PPY sheath grow without interruption and also prevents the mats to fold and swell when impregnated with water (Fig. S2).

Two more key factors determine the formation of a continuous and (macroscopically) homogeneous PPY sheath: the presence of a dopant-surfactant[42,47] and the polymerization rate, regulated by the temperature[40] and both Py and APS (oxidant) concentration[40,48] (refer to supporting information for more details). If Py polymerization goes fast, insoluble macroscopic PPY solid agglomerates will form (see Fig. S2), generating ultimately a not homogeneous nor continuous coating on the nanofibers, easily removed by washing. T must be maintained always near 4-5°C, since APS addition, to avoid this undesired drawback. If the oxidant concentration is too low, the mats will not be conductive: just not connected PPY domains will form on the fibers. Conversely, if the Py concentration is too high, solid, insoluble PPY domains will appear very soon (Fig. S2). DBSA ensures also the solubility of the forming PPY in water.[42] In the absence of DBSA, solid PPY black flakes will precipitate as soon as APS is added, even at T = 4°C (Fig. S2).

PAN@PPY/ZnO nanofibers

The subsequent immobilization of ZnO crystallites on the PAN@PPY nanofibers is described in Fig. 1. The formation of a nanometric ZnO coating, adherent on the fibers after washing and irradiation, requires a two-steps procedure (seeding and growing), in agreement with previous literature.[25,43]

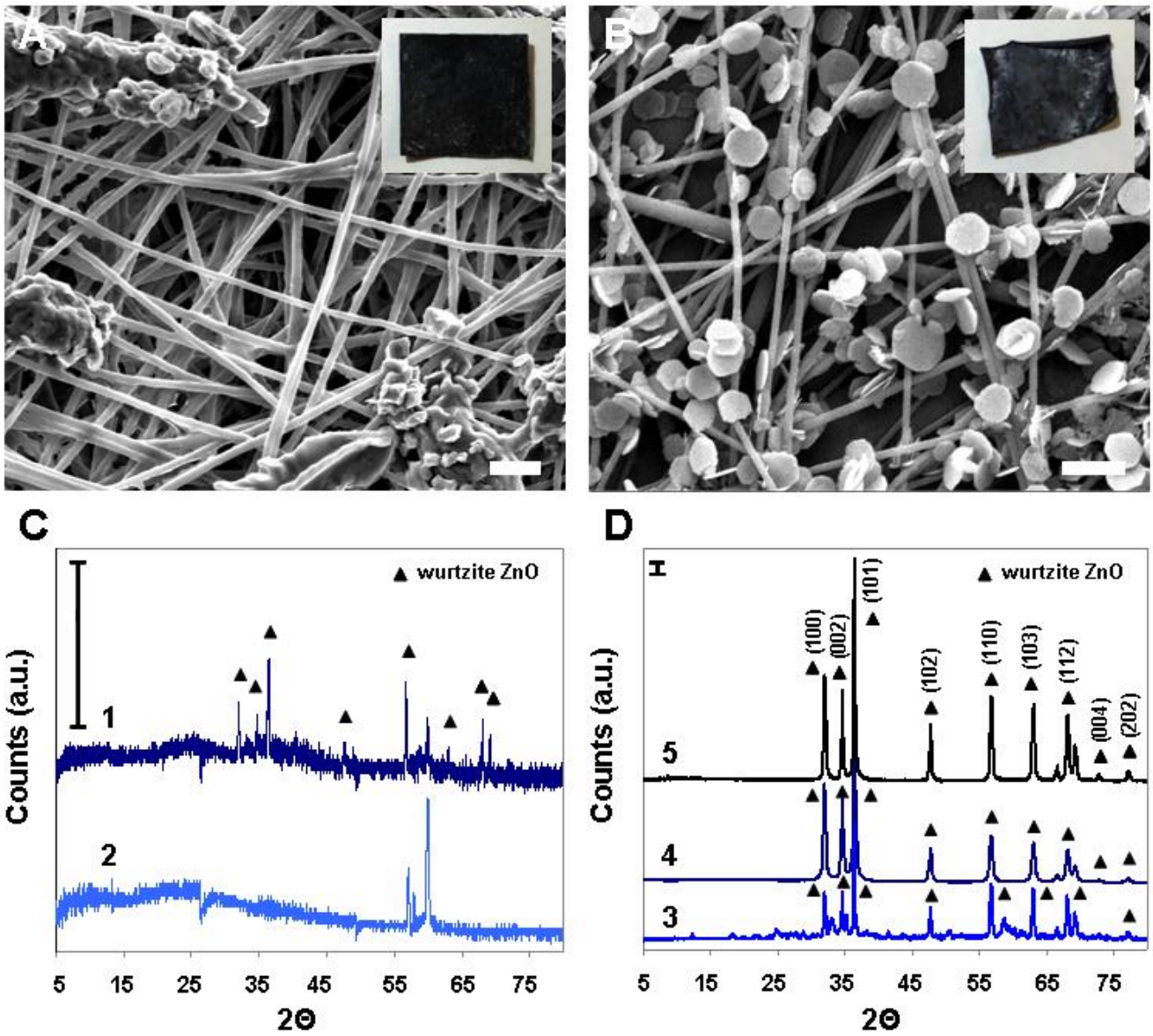

Figure 3: SEM micrographies of the PAN@PPY-seeds (A) and PAN@PPY/ZnO (B) samples, scale bars: 5 µm. X-ray diffractograms of (1) PAN@PPY/ZnO and (2) PAN@PPY mats, of (3) Zn-seeds, (4) ZnO_HT90 and (5) ZnO_HT180 powders, scale bars: 40 a.u. (D and E).

Fig. 3A represents the PAN@PPY mat after the seeding process, followed by curing at 100°C (PAN@PPY-seeds). A macroscopically homogeneous, white thin film adheres on the mat surface (see Fig. 3A inset, Fig. S7 and S8). It actually consists in a not homogeneous coverage of microscopic irregular aggregates (with size ranging from 10 to 100 µm, see also Fig. S9). The nanofiber surface, investigated through SEM microscopy, appears less rough compared to that of PAN@PPY. The increase in the average fiber thickness (1050 ± 200 nm) may not be related to the formation of a seeded nanolayer on the PPY sheath. After having been in contact with IPA, the nanofibers can partially swell, indeed.

After mild HT in the growing solution, the PAN@PPY-seeds mats result steadily coated with a white layer (Fig. 3B, inset). The seeds are dissolved or mostly converted in ZnO nanoplatelets, as shown in Fig. 3B. The average fiber thickness decreases remarkably (750 ± 100 nm) and their surface becomes smoother, because of the seeding layer dissolution and a partial shrinking/dissolution-degradation of the PPY coating. The HT partially degrades the semiconducting sheath but the drop in conductivity to $7 \cdot 10^{-3}$ S cm^{-1} (Fig. S4) is still acceptable.

XRD analysis on the complete system PAN@PPY/ZnO, compared to the PAN@PPY mat (Fig. 3D), allows to recognize the main characteristic peaks of the wurtzite hexagonal phase of ZnO (labelled with black triangles, reference peak list reported in SI).[49] The low peak intensity in the reported diffractograms is due to the thin oxide coating (the PAN@PPY/ZnO mats are 0.05-0.1 mm thick). The low signals prevent a clear identification of the chemical species and crystalline phases present in the white coatings on PAN@PPY-seeds and PAN@PPY/ZnO. We then refer to the Zn-seeds and ZnO_HT90 bulk powders, which correspond to the Zn-based phases formed on PAN@PPY during the seeding process and after the HT.

The X-ray diffraction pattern of the Zn-seeds powder (n.3, Fig. 3E) corresponds to the planes of the ZnO wurtzite structure (labelled with triangles) and highlights the presence of some impurities. The precursor used results mostly transformed in ZnO during the seed synthesis and curing step. The unconventional HT at low T (growing step), in the presence of HMTA as a source of OH^- and shape controller[50], converts completely the seeds in crystalline ZnO (ZnO_HT90 powder, Fig. 3E, n.4). Diffractogram n.5 refers to ZnO_HT180 powder, synthesized via a conventional HT (T = 180°C) and used, in this work, as a photocatalytic benchmark (see below). It is characterized by a pure, more crystalline (higher peak intensity), ZnO wurtzite phase, as well.

PAN@PPY mats must necessarily be coated first with a layer of ZnO seeds and cured. The PAN@PPY fibers treated just with the HT step (without seeding) result not steadily coated (unstable layer, detached right after washing, see Fig. S7). PAN@PPY mats, after the seeding cycles and the mild HT, without previous curing at 100°C, own the same unstable ZnO coating.

Photocatalytic activity

Fig. 4 reports the material photoactivity, assessed through photodegradation of MO in water, under UVA light. The MO degradation rate, in the presence of the various control samples, allows to understand the contribution of the different layers to the overall photocatalytic activity of the combined system PAN@PPY/ZnO. All the materials exhibit negligible dye adsorption in dark, before photodegradation. The PAN@PPY mats do not show any photoactivity, since the MO abatement in their presence is equal to direct photolysis. PAN/ZnO, a reference system with ZnO grown on insulating PAN nanofibers, is able to abate, on average, the 34% of the original concentration. The ZnO coating appears as the key component for the system photoactivity. However, PAN/ZnO photodegradation rate is remarkably lower compared to PAN@PPY/ZnO, which abates the 80% of MO, on average. The semiconducting PPY layer results then crucial to the overall performance of the complete system.

The last reference material tested, ZnO_HT180, is a not supported nanopowder. The ZnO_HT180 slurry used in the photodegradation tests contains the same amount of ZnO present on the PAN@PPY/ZnO mats, estimated from thermogravimetric analysis (0.4 g of oxide per gram of fiber, see Fig. S10). ZnO_HT180 is able to induce a complete MO photodegradation. It probably owns a higher exposed surface area, since it is not immobilized on a support. Nevertheless, the lower photocatalytic activity of PAN@PPY/ZnO resides most likely in the less crystalline ZnO synthesized on the mats, because of the HT at

lower T (as shown by XRD in Fig. 3E). HT at higher T remarkably degrades the PPY coverage and progressively compromises the PAN mechanical properties. (Fig. S7)

The PAN@PPY/ZnO samples, tested in consecutive degradation cycles (Fig. 4), exhibit a remarkable photostability: the MO abatement decreases from 80% to 68% after five cycles (85% retention of the original photoactivity).

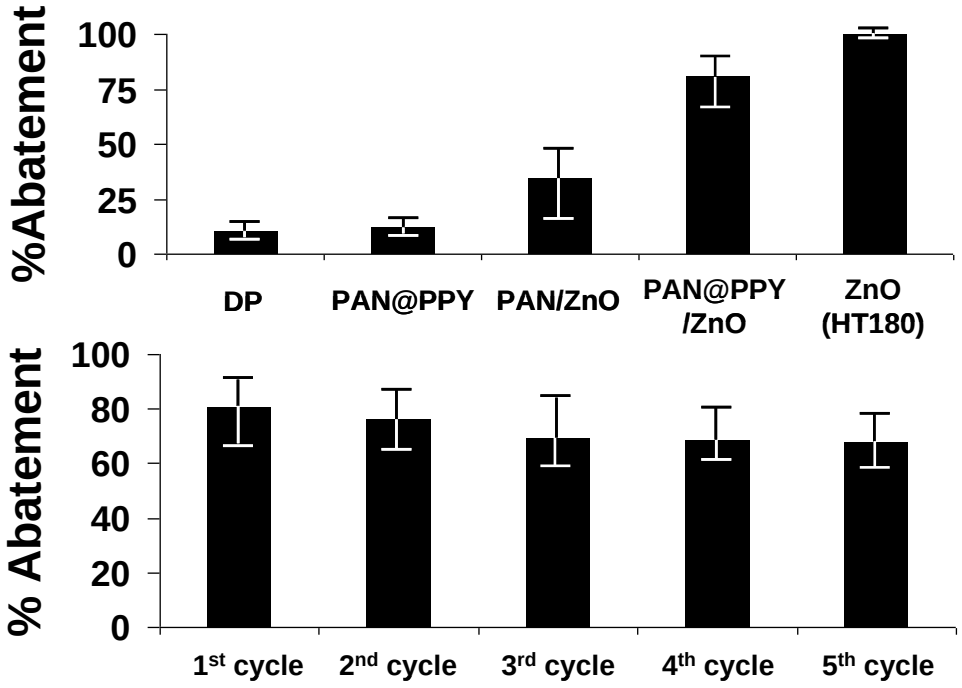

Figure 4: Percent of methyl orange (MO) abatement under UVA light. Top: from left to right, direct photolysis (DP), in the presence of PAN@PPY mat, PAN/ZnO mat (NO PPY), PAN@PPY/ZnO mat and a slurry of benchmark ZnO_HT180 nanopowder. Bottom: photodegradation cycles in the presence of PAN@PPY/ZnO.

The higher photoactivity of the complete system PAN@PPY/ZnO, compared to PAN/ZnO and PAN@PPY, resides primarily in the interaction, under irradiation, between PPY and ZnO. Electrochemical investigation of the PPY and ZnO layers, separately, allows to clarify the nature of this interaction.

Chronopotentiometric dark-light cycles and cyclic voltammetries carried out on Zn-seeds and ZnO_HT90 (Fig. S11) confirm that the two materials are very similar. Their conduction band position is very close (estimated around -0.8 V vs Ag/AgCl), so is their Fermi potential, in dark and under irradiation. The photopotential developed under irradiation by the Zn-seed powder is slightly lower (250 mV, in the case of ZnO_HT90 it is >300 mV) and the recombination of its photogenerated charges is faster than ZnO_HT90 (faster recovery of the potential values in dark, after irradiation interruption), as a consequence of the lower crystallinity and purity. The same measurements on PPY show that it is a p-type (open circuit potential shifting toward more positive values under irradiation), very low band gap semiconductor (conduction and valence band potentials estimated respectively around -0.3 V and +0.1 V vs Ag/AgCl, by cyclic voltammetry).

In accordance with the measured band energies of ZnO and PPY, a type-I p-n heterojunction forms between the PPY sheath and the ZnO nanocrystals, as reported in Fig. 5. The photoelectrons generated under irradiation on ZnO, at the interface with PPY, are partially collected on the PPY surface and then quenched by molecular oxygen, to form the superoxide radical anion $O_2^{\bullet -}$. It then reduces directly the dye or converts in H_2O_2[18], a reactive chemical specie often employed during advanced water decontamination

treatments.[13] The holes formed in the ZnO valence band directly oxidize the MO dye or react with OH^- to form the $OH^\bullet$ radical[49], which is further able to oxidize MO and any dissolved organic contaminant, thanks to its extremely high oxidative potential. The formed heterojunction inhibits the recombination of the photoinduced electrons and holes, by promoting their selective collection on PPY and on ZnO, respectively, becoming then responsible for the observed enhancement in photoactivity.

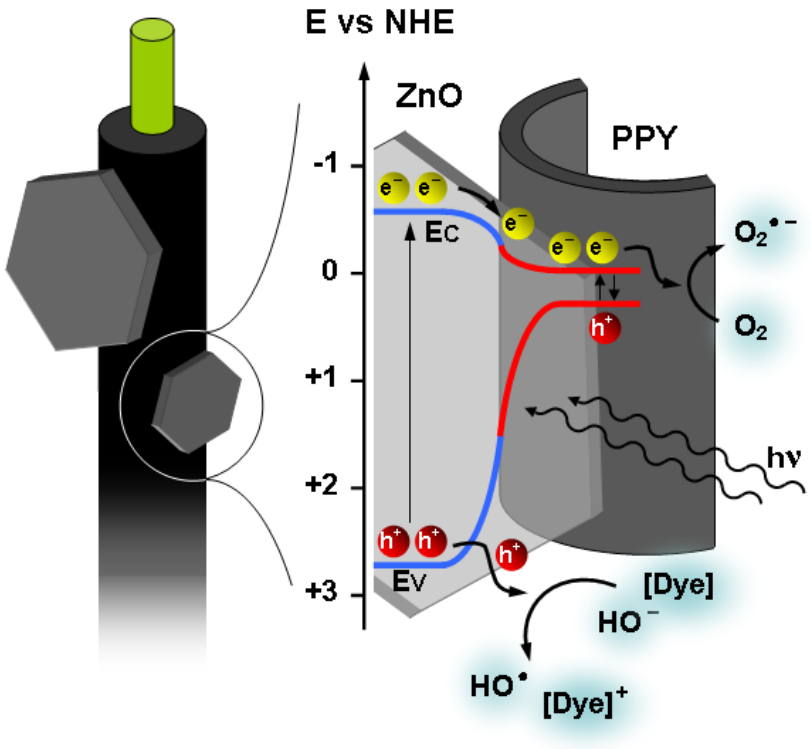

Figure 5: Band diagram of the type-I heterojunction formed between the ZnO nanocrystals and the PPY sheath together with the processes happening under UVA irradiation and the main chemical reactions at the interface between the PAN@PPY/ZnO mat and the MO/treatment solution. Band energies were measured in aqueous solution, at pH=9 (Fig. S11) and here reported vs NHE reference.

CONCLUSIONS AND OUTLOOK

We designed and optimized the preparation of a photoactive system where electrospun semiconducting nanofibers are supporting a photoactive metal oxide layer. The combination of a conducting polymer, PPY, and a n-type oxide, ZnO, resulted in the enhancement of the photocatalytic activity, thanks to the formation of a heterojunction at the interface between the two active materials.

The nanofibers production is scalable: all the chemicals employed are not expensive, the polymerization of PPY is carried out in water, in air, easier and “green” conditions compared to many other conducting polymers, where organic solvents and inert atmosphere are required.

Water affinity of the electrospun PAN mats dramatically increases after ozonation. It allows the growth of a continuous PPY nanosheath, steadily adherent on the PAN surface, stable after washing and the mild HT. T must be kept at 4-5°C during the whole PAN@PPY preparation, to slow down the Py polymerization rate and favour the formation of a (macroscopically) homogeneous PPY layer. A two-steps mechanism (a seeding step followed by a HT at 90°C) is necessary to form the crystalline ZnO coating, stable after washing and irradiation, while preserving the polymeric semiconducting support. Further

improvements will concern the increase of the system photoactivity, attainable mainly through a more crystalline oxide phase.

This approach paves the way for the design of new coupled materials. On one side, electrospun semiconducting PAN@PPY nanofibers can be decorated with other photoactive oxides[26,51,52], i.e. hematite, TiO_2 and WO_3. Alternative synthetic methods requiring mild conditions are also available to generate new oxide coatings, for example electrodeposition (exploiting the PPY layer conductivity). On the other side, different conducting/semiconducting fibers, more resistant to harsh synthetic conditions, can support more crystalline ZnO (or other photoactive oxides, i.e. TiO_2). Despite conductive carbon nanofibers have been recently employed[53,54], semiconducting flexible nanofibers are still lacking.

These hybrid systems can be applied in advanced oxidation processes, for decontamination of water containing emerging persistent pollutants. Chemical sensing represents another possible field of application.[22] Many molecules of common interest (gaseous NH_3, NO_X, dissolved metallic ions..) are able to reduce/oxidize on the mat surface, under irradiation.[52] The consequent alteration of the mat conductivity/impedance can be detected and quantified. Differently from other common sensing systems, the combined mats here presented own a high surface area, are flexible, self standing and can be easily prepared large in size. These properties make them promising/suitable for future applications on a wide scale.

REFERENCES

1. M. Schiavello, Photocatalysis and environment: trends and applications, Kluwer, Dordrecht, 1988. ISBN: 9027727600 9789027727602.
2. N. Serpone, E. Pelizzetti, Photocatalysis: fundamentals and applications, Wiley, New York, 1989. ISBN: 0471626031 9780471626039.
3. M. H. Sui, L. She, Review on research and application of mesoporous transitional metal oxides in water treatment, *Front. Env. Sci. Eng.* **2013** (7) 795-802.
4. D. S. Bhatkhande, V. G. Pangarkar, A. A. C. M. Beenackers, Photocatalytic degradation for environmental applications – a review, **2002** (77) 102-116.
5. C. Minero, V. Maurino, D. Vione, Photocatalysis and Water Purification: From Fundamentals to Recent Applications - Photocatalytic Mechanisms and Reaction Pathways Drawn from Kinetic and Probe Molecules, pp. 53-72, Wiley-VCH, Weinheim, 2013. ISBN: 9783527331871.
6. U. I. Gaya, A. H. Abdullah, Heterogeneous photocatalytic degradation of organic contaminants over titanium dioxide: A review of fundamentals, progress and problems, *J. Photochem. Photobiol. C* **2008** (9) 1-12.
7. K. M. Lee, C. W. Lai, K. S. Ngai, J. C. Juan, Recent developments of zinc oxide based photocatalyst in water treatment technology: A review, *Water Res* **2016** (88) 428-448.
8. M. A. M. Adnan, N. M. Julkapli, S. B. A. Hamid, Review on ZnO hybrid photocatalyst: impact on photocatalytic activities of water pollutant degradation, *Rev. Inorg. Chem.* **2016** (36) 77-104.
9. Y. Xia, J. Wang, R. S. Chen, D. L. Zhou, L. Xiang, A Review on the Fabrication of Hierarchical ZnO Nanostructures for Photocatalysis Application, *Crystals* **2016** (6) 148.
10. J.-L. Wang, P.-Y. Yang, M.-H. Juang, T.-Y. Hsieh, C.-C. Hwang, C.-P. Juan, I. C. Lee, Zinc oxide thin-film transistors fabricated via low-temperature hydrothermal method, *Surf. Coat. Technol.* **2013** (231) 428-432.
11. J. J. Richardson, F. F. Lange, Controlling Low Temperature Aqueous Synthesis of ZnO. 1. Thermodynamic Analysis, *Cryst. Growth Des.* **2009** (9) 2570-2575.
12. H. Dong, G. Zeng, L. Tang, C. Fan, C. Zhang, X. He, Y. He, An overview on limitations of TiO2-based particles for photocatalytic degradation of organic pollutants and the corresponding countermeasures, *Water Res.* **2015** (79) 128-146.

13. O. M. Rodriguez-Narvaez, J. M. Peralta-Hernandez, A. Goonetilleke, E. R. Bandala, Treatment technologies for emerging contaminants in water: A review, *Chem. Eng. J.* **2017** (323) 361-380.
14. X. Qu, P. J. J. Alvarez, Q. Li, Applications of nanotechnology in water and wastewater treatment, *Water Res.* **2013** (47) 3931-3946.
15. H. K. Shon, S. Phuntsho, D. S. Chaudhary, S. Vigneswaran, J. Cho, Nanofiltration for water and wastewater treatment – a mini review, *Drink. Water Eng. Sci.* **2013** (6) 47-53.
16. S. Tul Muntha, A. Kausar, M. Siddiq, Advances in Polymeric Nanofiltration Membrane: A Review, *Polym. Plast. Technol. Eng.* **2016** (56) 841-856.
17. S. Mozia, Photocatalytic membrane reactors (PMRs) in water and wastewater treatment. A review, *Sep. Purif. Technol.* **2010** (73) 71-91.
18. M. Sarro, N. P. Gule, E. Laurenti, R. Gamberini, M. C. Paganini, P. E. Mallon, P. Calza, ZnO-based materials and enzymes hybrid systems as highly efficient catalysts for recalcitrant pollutants abatement, *Chem. Eng. J.* **2018** (334) 2530-2538.
19. A. Haider, S. Haider, I.-K. Kang, A comprehensive review summarizing the effect of electrospinning parameters and potential applications of nanofibers in biomedical and biotechnology, *Arab. J. Chem.* **2018** (11) 1165-1188.
20. C. Y. Lee, S. Y. Li, P. Lin, T. Y. Tseng, ZnO Nanowires Hydrothermally Grown on PET Polymer Substrates and Their Characteristics, *J. Nanosci. Nanotechnol.* **2005** (5) 1088-1094.
21. X. Shi, W. Zhou, D. Ma, Q. Ma, D. Bridges, Y. Ma, A. Hu, Electrospinning of Nanofibers and Their Applications for Energy Devices, *J. Nanomater.* **2015** (2015) 1-20.
22. B. Ding, M. Wang, X. Wang, J. Yu, G. Sun, Electrospun nanomaterials for ultrasensitive sensors, *Mater. Today* **2010** (13) 16-27.
23. T. S. He, Z. F. Zhou, W. B. Xu, F. M. Ren, H. H. Ma, J. Wang, Preparation and photocatalysis of TiO2-fluoropolymer electrospun fiber nanocomposites, *Polymer* **2009** (50) 3031-3036.
24. F. Kayaci, S. Vempati, C. Ozgit-Akgun, N. Biyikli, T. Uyar, Enhanced photocatalytic activity of homoassembled ZnO nanostructures on electrospun polymeric nanofibers: A combination of atomic layer deposition and hydrothermal growth, *Appl. Catal. B: Environ.* **2014** (156) 173-183.
25. Z. J. Chang, "Firecracker-shaped" ZnO/polyimide hybrid nanofibers via electrospinning and hydrothermal process, *Chem. Commun.* **2011** (47) 4427-4429.
26. S. J. A. Moniz, S. A. Shevlin, D. J. Martin, Z.-X. Guo, J. Tang, Visible-light driven heterojunction photocatalysts for water splitting – a critical review, **2015** (8) 731-759.
27. C. Janáky, K. Rajeshwar, The role of (photo)electrochemistry in the rational design of hybrid conducting polymer/semiconductor assemblies: From fundamental concepts to practical applications, *Prog. Polym. Sci.* **2015** (43) 96-135.
28. Y. Li, J. Gong, M. McCune, G. He, Y. Deng, I–V characteristics of the p–n junction between vertically aligned ZnO nanorods and polyaniline thin film, *Synthetic Metals* **2010** (160) 499-503.
29. J. L. Brédas, B. Thémans, J. M. André, Bipolarons in polypyrrole chains, *Phys. Rev. B* **1983** (27) 7827-7830.
30. T.-H. Le, Y. Kim, H. Yoon, Electrical and Electrochemical Properties of Conducting Polymers, *Polymers-Bassel* **2017** (9) 150.
31. K. R. Reddy, M. Hassan, V. G. Gomes, Hybrid nanostructures based on titanium dioxide for enhanced photocatalysis, *Appl. Catal. A: Gen.* **2015** (489) 1-16.
32. Y. C. Ding, F. Zheng, Z. T. Zhu, Low-temperature seeding and hydrothermal growth of ZnO nanorod on poly(3,4-ethylene dioxythiophene):poly(styrene sulfonic acid), *Mater. Lett.* **2016** (183) 197-201.
33. J. Y. Lee, C. A. Bashur, A. S. Goldstein, C. E. Schmidt, Polypyrrole-coated electrospun PLGA nanofibers for neural tissue applications, *Biomaterials* **2009** (30) 4325-4335.
34. F. J. Miao, C. L. Shao, X. H. Li, K. X. Wang, Y. C. Liu, Flexible solid-state supercapacitors based on freestanding nitrogen-doped porous carbon nanofibers derived from electrospun polyacrylonitrile@polyaniline nanofibers, *J. Mater. Chem. A* **2016** (4) 4180-4187.
35. I. S. Chronakis, S. Grapenson, A. Jakob, Conductive polypyrrole nanofibers via electrospinning: Electrical and morphological properties, *Polymer* **2006** (47) 1597-1603.
36. R. Balint, N. J. Cassidy, S. H. Cartmell, Conductive polymers: Towards a smart biomaterial for tissue engineering, *Acta Biomater.* **2014** (10) 2341-2353.

37. T. S. Kang, S. W. Lee, J. Joo, J. Y. Lee, Electrically conducting polypyrrole fibers spun by electrospinning, *Synthetic Metals* **2005** (153) 61-64.
38. A. Laforgue, L. Robitaille, Fabrication of poly-3-hexylthiophene/polyethylene oxide nanofibers using electrospinning, *Synthetic Metals* **2008** (158) 577-584.
39. Y. Shi, Y. Li, J. Zhang, Z. Yu, D. Yang, Electrospun polyacrylonitrile nanofibers loaded with silver nanoparticles by silver mirror reaction, *Mater. Sci. Eng. C* **2015** (51) 346-355.
40. S. Rapi, V. Bocchi, G. P. Gardini, Conducting Polypyrrole by Chemical Synthesis in Water, *Synthetic Metals* **1988** (24) 217-221.
41. U. Lange, N. V. Roznyatovskaya, V. M. Mirsky, Conducting polymers in chemical sensors and arrays, *Anal. Chim. Acta* **2008** (614) 1-26.
42. Y. Q. Shen, M. X. Wan, In situ doping polymerization of pyrrole with sulfonic acid as a dopant, *Synthetic Metals* **1998** (96) 127-132.
43. T. J. Athauda, U. Butt, R. R. Ozer, One-dimensional hierarchical composite materials based on ZnO nanowires and electrospun blend nanofibers, *RSC Adv.* **2013** (3) 21431-21438.
44. A. Kołodziejczak-Radzimska, T. Jesionowski, Zinc Oxide-From Synthesis to Application: A Review, *Materials* **2014** (7) 2833-2881.
45. H. Hayashi, Y. Hakuta, Hydrothermal Synthesis of Metal Oxide Nanoparticles in Supercritical Water, *Materials* **2010** (3) 3794-3817.
46. S. Roth, D. Carroll, W. John, Sons, One-dimensional metals: conjugated polymers, organic crystals, carbon nanotubes, Second ed., Wiley-VCH, Weinheim; Chichester, 2004. ISBN: 3527307494 9783527307494.
47. D. C. Trivedi, Influence of counter ion on polyaniline and polypyrrole, *Bull. Mater. Sci.* **1999** (22) 447-455.
48. K. C. Khulbe, R. S. Mann, C. P. Khulbe, Polymerization of pyrrole by potassium persulfate, *J. Polym. Sci. Pol. Chem.* **1982** (20) 1089-1095.
49. E. Cerrato, C. Gionco, I. Berruti, F. Sordello, P. Calza, M. C. Paganini, Rare earth ions doped ZnO: Synthesis, characterization and preliminary photoactivity assessment, *J. Solid State Chem.* **2018** (264) 42-47.
50. R. Parize, J. Garnier, O. Chaix-Pluchery, C. Verrier, E. Appert, V. Consonni, Effects of Hexamethylenetetramine on the Nucleation and Radial Growth of ZnO Nanowires by Chemical Bath Deposition, *J. Phys. Chem. C* **2016** (120) 5242-5250.
51. L. Geng, S. Wu, Preparation, characterization and gas sensitivity of polypyrrole/γ-Fe2O3 hybrid materials, *Mater. Res. Bull.* **2013** (48) 4339-4343.
52. J. H. Sun, X. Shu, Y. L. Tian, Z. F. Tong, S. L. Bai, R. X. Luo, D. Q. Li, A. F. Chen, Preparation of polypyrrole@WO3 hybrids with p-n heterojunction and sensing performance to triethylamine at room temperature, *Sensor. Actuat. B-Chem.* **2017** (238) 510-517.
53. J. Chen, D. Yu, W. Liao, M. Zheng, L. Xiao, H. Zhu, M. Zhang, M. Du, J. Yao, WO3–x Nanoplates Grown on Carbon Nanofibers for an Efficient Electrocatalytic Hydrogen Evolution Reaction, *ACS Appl. Mater. Interfaces* **2016** (8) 18132-18139.
54. Y. Liu, Q. Huang, G. Jiang, D. Liu, W. Yu, Cu2O nanoparticles supported on carbon nanofibers as a cost-effective and efficient catalyst for RhB and phenol degradation, *J. Mater. Res.* **2017** (32) 3605-3615.